

AD-A254 291



## NTATION PAGE

Form Approved  
OMB No. 0704-0188

Estimated to average 1 hour per response, including the time for reviewing instructions, searching existing data sources, gathering and maintaining the data needed, and completing and reviewing the collection of information. Send comments regarding this burden estimate or any other aspect of the burden to Washington Headquarters Services, Directorate for Information Operations and Reports, 1215 Jefferson Avenue, Washington, DC 20301.

1. AGENCY USE ONLY (Leave Blank)	2. REPORT DATE	3. REPORT TYPE AND DATES COVERED	
	27 July 1992	Final Technical, 1 Dec 88 - 30 Nov 91	
4. TITLE AND SUBTITLE		5. FUNDING NUMBERS	
State-Resolved Reaction Dynamics		TA 2303/B1 <i>(2)</i>	
6. AUTHOR(S)		AFOSR-TR-92-0192	
Richard N. Zare			
7. PERFORMING ORGANIZATION NAME(S) AND ADDRESS(ES)		8. PERFORMING ORGANIZATION REPORT NUMBER	
Department of Chemistry Stanford University Stanford, CA 94305		SPO# 6871	
9. SPONSORING/MONITORING AGENCY NAME(S) AND ADDRESS(ES)		10. SPONSORING/MONITORING AGENCY REPORT NUMBER	
Air Force Office of Scientific Research Building 410, Room B219 Bolling AFB, DC 20332-6448		AFOSR-89-0264	
11. SUPPLEMENTARY NOTES		DTIC ELECTE AUG 21 1992 SAD	
None		12b. DISTRIBUTION STATEMENT	
Approved for public release; Distribution is unlimited		A	
13. ABSTRACT (Maximum 200 words) This research effort is comprised of two groups of experiments. The first group measures and characterizes the electron ejected in a photoionization event. The second group is concerned with understanding the role of energy in affecting the outcome of ion-molecule reactions. High resolution, angle-resolved photoelectron spectroscopy was carried out following resonance enhanced multiphoton ionization (REMPI) of nitric oxide. These measurements have led to a "complete" description of this photoionization event. Photoelectron spectroscopy was also used to measure the degree of vibrational state-selectivity resulting from REMPI of NH <sub>3</sub> and HBr/DBr. Additionally, the rotational state distributions resulting from HBr/DBr/HCl REMPI were measured using LIF. These state distributions were used in the study of the near resonant charge transfer reaction of DBr <sup>+</sup> + HBr, where the reagent ion was state-selectively prepared with REMPI and the product state distributions were monitored with LIF. vibrationally state-selected ammonia ions generated by REMPI were used to investigate the effect of kinetic and vibrational energy in determining the product formation tendencies of the reaction NH <sub>3</sub> <sup>++</sup> ND <sub>3</sub> . Measurement of the product cross sections has shown the differing effects of vibrational and translational excitation on dynamics of this ion-molecule system.			
14. SUBJECT TERMS		15. NUMBER OF PAGES	
Resonance-enhanced multiphoton ionization (REMPI), photoelectrons, photoionization dynamics, laser-induced fluorescence, ion-molecule reactions			
16. PRICE CODE			
17. SECURITY CLASSIFICATION OF REPORT	18. SECURITY CLASSIFICATION OF THIS PAGE	19. SECURITY CLASSIFICATION OF ABSTRACT	20. LIMITATION OF ABSTRACT
Unclassified	Unclassified	Unclassified	UL

### Objective of Research

This research effort is directed toward improving our understanding of highly reactive molecular species; during this grant period work has focused exclusively on gas phase charged molecules. We are investigating in detail the nature and reactivity of these species. Multiphoton ionization, an integral part of this work, is being used to probe the dynamics of photoionization and to generate state-selected ions. These state-selected ions then serve as reagents in ion-molecule reactions. This ability to prepare reagents in known initial states, when coupled with detailed measurements of the reaction products, provides unique insight into the role of vibrational and kinetic energy in determining the outcome of ion-molecule reactions. Such before and after measurements also allow inferences to be made concerning details of the reactive process dynamics.

### Status of the Research Effort

During this past grant period, we have continued our multifaceted investigation into the characteristics and chemistry of ionic species. The first set of experiments are studies of the photoelectron ejected in the ionization step of resonance-enhanced multiphoton ionization (REMPI). Characterization of the energy and anisotropy of this ejected electron provides information on the dynamics of the photoionization event for the NO molecule. The time-of-flight spectroscopy of these ejected electrons also provides the information necessary to ascertain the vibrational state of the resulting ion, which has been used to verify the state selective preparation by REMPI of a combination band excitation in  $\text{NH}_3^+$ . The second set of experiments study low energy (thermal) ion-molecule reactions of  $\text{H}(\text{D})\text{Br}^+$ , where REMPI is used to state-selectively prepare the reagent ion. Coupling this with state-selective product ion detection, state-to-state absolute thermal rate constants are determined. The third set of experiments study the role of vibrational excitation and kinetic energy in affecting the product intensities of the multichannel ion-molecule reaction  $\text{NH}_3^+ + \text{ND}_3$ . These high energy experiments (0.5-10 eV center-of-mass) again utilize REMPI to state-selectively prepare the reagent ion. The details and results of these experiments are discussed on the following pages.

92-23282



2 8 20 067

Approved for public release;  
distribution unlimited,

### A. Resonance-Enhanced Multiphoton Ionization-Photoelectron Spectroscopy (REMPI-PES)

We have studied the photoelectron spectroscopy of several small molecules employing a time-of-flight (TOF) photoelectron spectrometer used in conjunction with REMPI of jet cooled molecules. In these experiments we have pursued two objectives: the characterization of the ion states selected in the REMPI processes, and a detailed study of the photoionization dynamics of the NO molecule.

Photoelectron spectroscopy provides a unique source of information concerning the ion states that are formed from photoionization processes. Although in some cases these states can be probed by optical methods, photoelectron spectroscopy is a more direct means to accomplish this goal. Using the energy conservation relation

$$E_{int,mol} + h\nu = E_{int,ion} + K_e \quad (1),$$

we can deduce the internal states of the ion formed by measuring the photoelectron kinetic energy. In equation (1),  $E_{int,mol}$  represents the internal energy of the molecules to be photoionized,  $E_{int,ion}$  the internal energy of the ion formed, and  $K_e$  the kinetic energy of the photoelectron. In this regard we have determined the spin-orbit and vibrational states populated upon ionization of state-selected  $5p\pi$  Rydberg states of HBr/DBr and the vibrational states populated upon ionization of NO via the C  $^2\Pi$  state.<sup>1</sup> We have also determined the vibrational states populated upon ionization of ammonia via several vibrational states of the C' Rydberg state (Fig. 1). The information we have obtained in these experiments has proved essential to various studies such as ion-molecule reaction dynamics of state-selected ions.

Regarding the second objective, we have also studied the photoionization dynamics of NO via the A  $^2\Sigma^+$  state. Using REMPI we are able to ionize molecules from a well-defined quantum level in a chosen intermediate electronic state. Our TOF spectrometer provides enough energy resolution to determine the high J ion rotational state associated with each photoelectron (Fig. 2). In addition, because our spectrometer is field free, we can determine the photoelectron angular distributions associated with each rotational branch. We have determined the energy-resolved photoelectron angular distributions (PADs) following the photoionization of NO via the v=1, N=22 rovibrational level of the A  $^2\Sigma^+$  state.<sup>2</sup> In conjunction with our experimental work, we have also derived a general expression that describes the PAD following (1+1') REMPI of a molecule with linearly polarized light beams.<sup>3</sup> By performing high resolution, angle resolved photoelectron spectroscopy and fitting the experimental results to the model, we have obtained the most detailed information about the photoionization dynamics of NO.

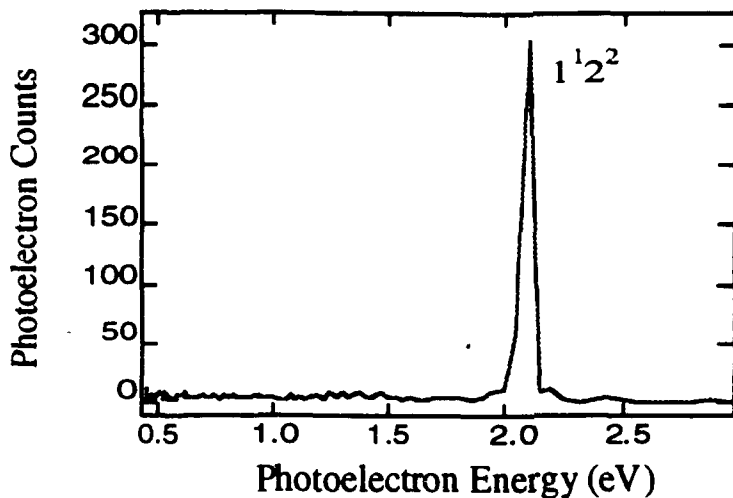


**Figure 1:** Photoelectron TOF spectrum for (2+1) REMPI of  $\text{NH}_3$  via  $1^12^2$  combination band of the  $\tilde{\text{C}}'$  Rydberg state.

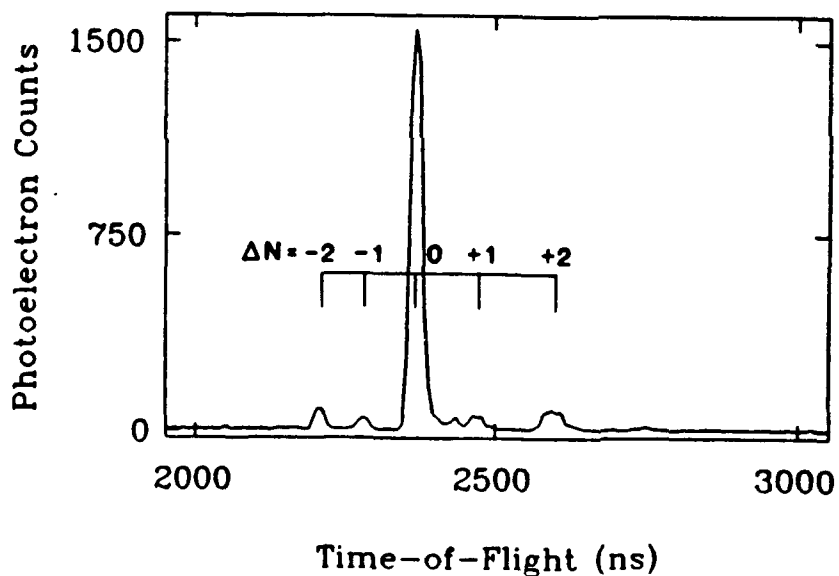


**Figure 2.** Photoelectron TOF spectrum for (1+1') REMPI of NO via the  $P_{21}+Q_1(22.5)$  transition to the  $A\ 2\Sigma^+$  ( $v_i=1$ ,  $N_i=22$ ) level with  $\theta_T=0$ .

In (1+1') REMPI employing two linearly polarized lasers with the angle  $\theta_T$  between the polarization vectors, the PAD can be expressed by<sup>3</sup>

$$I(\theta, \phi) = \beta_{00} Y_{00}(\theta, \phi) + \sum_{L=2,4} \sum_{M=-2}^2 \beta_{LM} Y_{LM}(\theta, \phi) \quad (2).$$

Here  $\beta_{LM}$  coefficients contain the dynamical information, i.e., the radial electric dipole matrix elements that connect the electronic wave function of the intermediate state to the outgoing partial waves, in addition to the geometrical quantities. By fitting the experimental PAD's to the above equation, we have been able to obtain the dynamical parameters that are needed to describe the photoionization process under study.<sup>2</sup> The dynamical parameters determined from the fit were found to agree reasonably well with the result of an *ab initio* calculation for the same process carried out by Rudolph and McKoy.<sup>4</sup> There exists, however, some discrepancies between the experiments and theoretical calculations, which may indicate the need to refine the theory, for example, by including electron correlation effects.

One of the important features of our formalism is that once we determine the dynamical parameters, we are able to use them to predict the various characteristics of a given rotational level of the ion from which the photoelectron has departed.<sup>3</sup> By measuring the PAD we observe the alignment of the photoelectron orbital angular momentum. From this observation, we can deduce the alignment of the ion since the alignments of the intermediate state and the ionizing photon are known.

We now have a general formalism that describes the (1+1') REMPI of a molecule when the linear polarization vectors of the resonant and ionizing lasers are at any angle. More importantly, we have demonstrated the power of this experimental technique; we have shown that REMPI-PES can provide a detailed insight into the photoionization dynamics in addition to information about the ion states formed from photoionization.

## B. State-to-State Ion-Molecule Reaction Dynamics

In our proposal, we speculated that it might be possible to study ion-molecule reaction dynamics in a bulb through the use of two pulsed dye lasers. This speculation has proven to be correct. Additionally, our preliminary work on probing the nascent distributions of ionized molecules has motivated the derivation of selection rules for the photoionization of diatomic molecules. In this section, we first describe the experimental work on ion-molecule reactions and then the theoretical work on selection rules.

### 1. Experimental Work

We have successfully investigated the state-to-state dynamics of the symmetric charge transfer reaction



using (2 + 1) REMPI to prepare selectively the ionic reagent  $\text{DBr}^+(2\Pi_i, v^+, J^+)$  and LIF to probe the product  $\text{HBr}^+(2\Pi_{i'}, v'^+, J'^+)$  state distribution. LIF spectra indicate that ionization through DBr Rydberg states prepares the reagent ion with over 98% purity in a particular spin-orbit state ( $i = 1/2, 3/2$ ) and vibrational state ( $v^+ = 0, 1$ ). With judicious selection of the two-photon transition to a particular rovibrational level of the DBr Rydberg state, reagent ions can be prepared with a limited number of populated rotational levels. Spectroscopic detection of products enables us to examine the distribution of product ions among the accessible vibrational, rotational, and spin-orbit levels as well as the  $\Lambda$ -doublet components of each rotational level. In this experiment, all of the energetically accessible product ion levels have been observed. In addition to the charge transfer channel, there is a second product channel, which cannot be detected by LIF:  $\text{DBr}^+ + \text{HBr} \rightarrow \text{DBrH}^+ + \text{Br}$ . Recently Viggiano has measured a rate of  $5.3 \times 10^{-10} \text{ cm}^3 \text{ sec}^{-1}$  for this channel.<sup>5</sup>

The experiment, illustrated in Figure 3, is performed in a flowing gas cell with the 1:2 DBr/HBr mixture held constant at a pressure of 15 mTorr. The LIF probe laser is delayed by 400 ns with respect to the REMPI laser to ensure that less than 10% of the reagent ions have undergone a single collision. A gated photomultiplier enables us to probe the very small product ion LIF signals by eliminating the fluorescence background arising from the intense REMPI laser. This device improves the signal-to-noise ratio by at least an order of magnitude. The LIF signal is normalized with respect to the power of the LIF laser and the number of reagent ions formed by REMPI. All LIF spectra of  $\text{DBr}^+$  and  $\text{HBr}^+$  were obtained by excitation to the  $v = 0$  level of the  $A \ ^2\Sigma^+$  state so that the Franck-Condon factors could be used to convert LIF line strengths to relative populations.

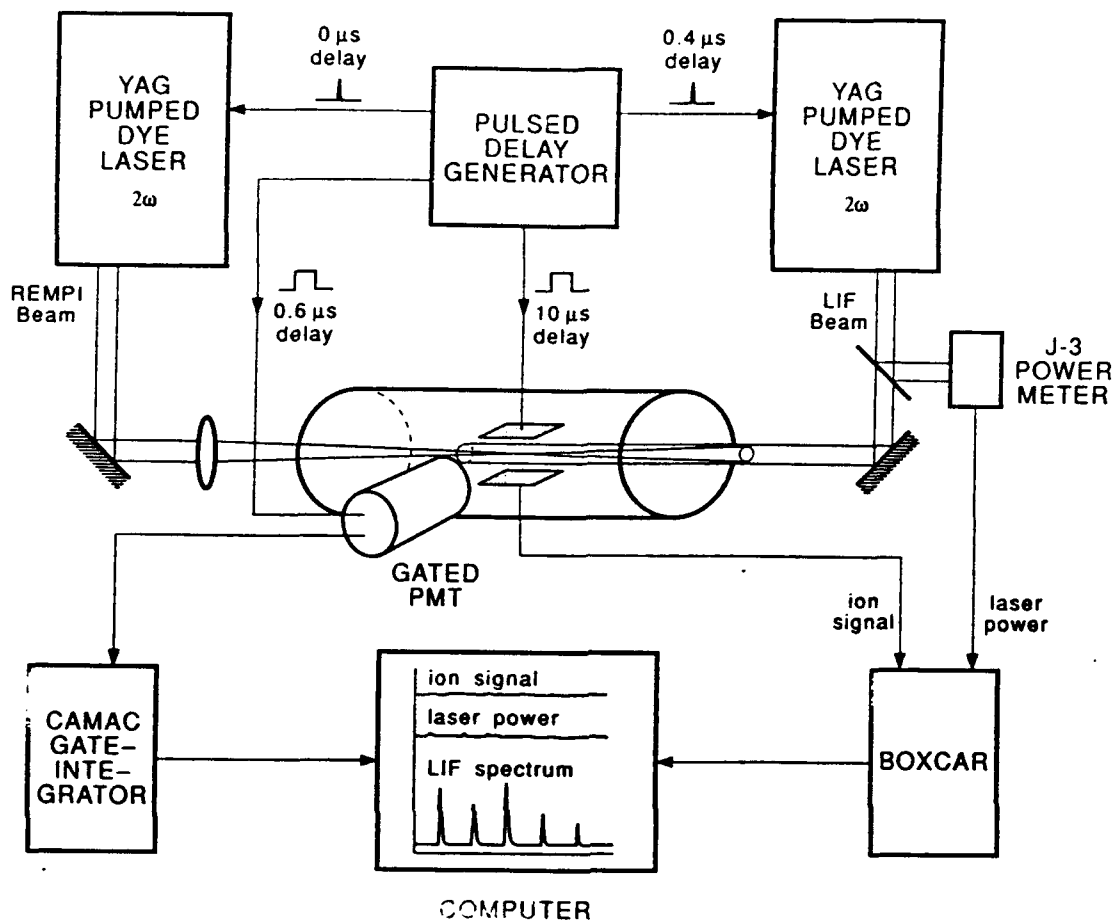


**Figure 3:** Experimental set-up used to study the charge transfer reaction  $\text{DBr}^+ + \text{HBr}$  in a bulb.

We have observed that the charge transfer reaction of  $\text{DBr}^+ 2\Pi_{3/2}, v^+ = 0$  and 1 with a thermal distribution of  $\text{HBr}$  yields  $\text{HBr}^+ 2\Pi_{3/2}, v^+=0$ , whereas the reaction of  $\text{DBr}^+ 2\Pi_{1/2}, v^+=0$  and 1 with  $\text{HBr}$  yields  $\text{HBr}^+$  in the  $2\Pi_{1/2}, v^+=0$  and  $2\Pi_{3/2}, v^+=0$  and 1 levels; see the energy level diagram in Figure 4 for details. With these data for the symmetric charge transfer reaction (4), it is possible to construct a full-scale state-to-state reaction channel matrix.<sup>6</sup> The ability to monitor both the initial state distribution of the  $\text{DBr}^+$  reagent and the final state distribution of the product  $\text{HBr}^+$  arising from a particular initial state distribution (Figure 5) under the same experimental conditions permits determination of the state-to-state reaction rates,  $R_{i \rightarrow j}$ .

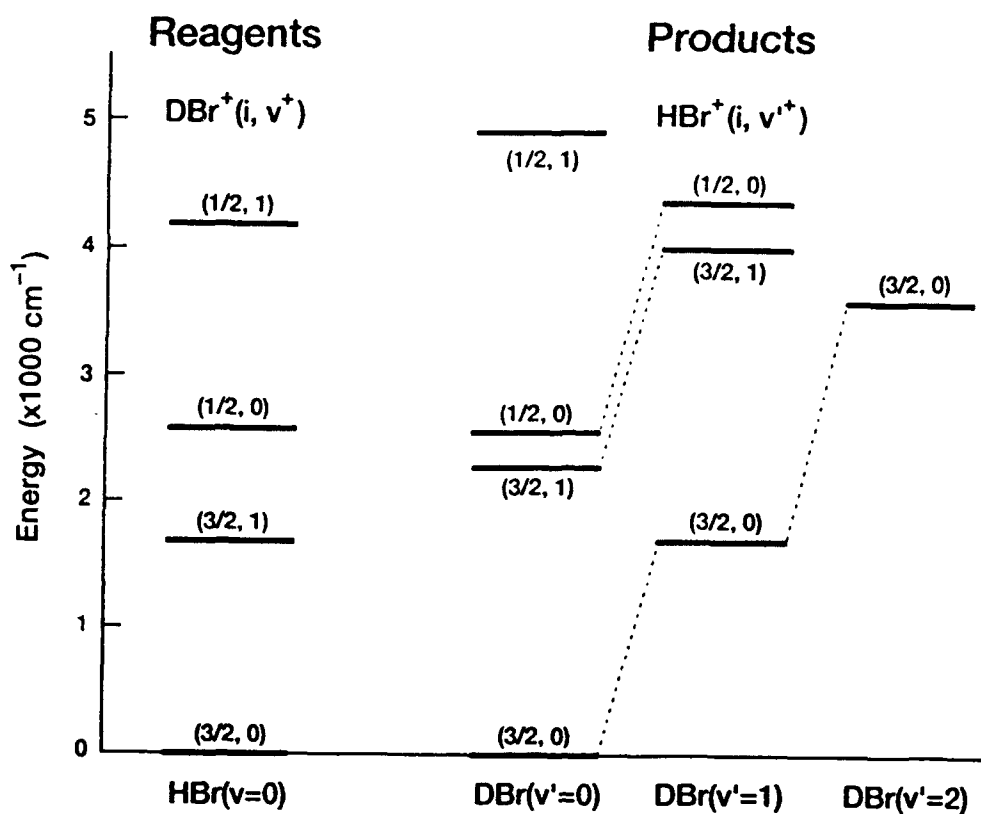


**Figure 4:** The energy level diagrams of  $\text{DBr}^+$  and  $\text{HBr}^+$ . The reaction channels have been indicated for the reaction of  $\text{DBr}^+(2\Pi_{1/2} \, v=0) + \text{HBr}$  to possible  $\text{HBr}^+$  states.

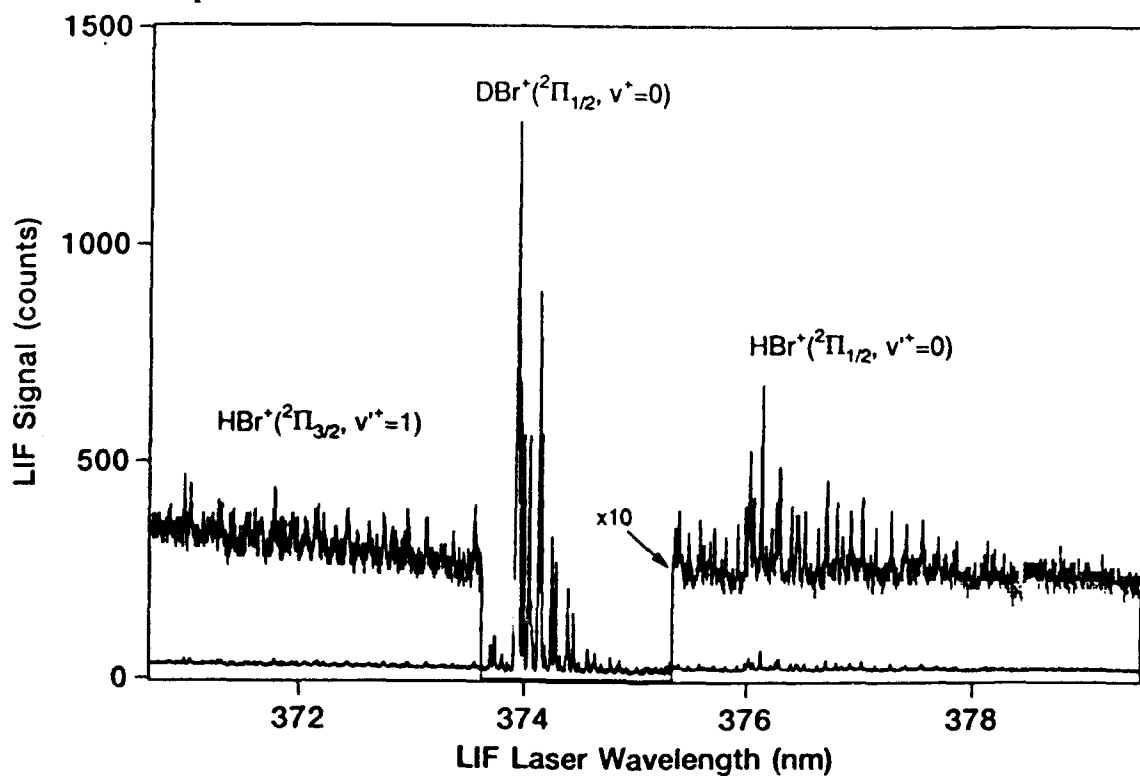


**Figure 5:** The spectrum of reagent  $\text{DBr}^+$  and product  $\text{HBr}^+$  obtained by pumping  $\text{DBr}^+ 2\Pi_{1/2} \, v=0$  state in a 2:1 HBr and DBr mixture of total pressure 15 mTorr.

In this experiment the reaction time is simply the time delay between the REMPI laser and the LIF laser. Evaluation of the equation

$$R_{i \rightarrow j} = k_{i \rightarrow j} N_{HBr} \quad (4)$$

where  $R_{i \rightarrow j}$  is the experimentally determined reaction rate and  $N_{HBr}$  is the molecular density of HBr, yields the state-to-state absolute reaction rate constant  $k_{i \rightarrow j}$ . We find that the rate constant  $k_{1/2, v=0 \rightarrow 1/2, v=0} = 1.5 \times 10^{-10} \text{ cm}^3 \text{sec}^{-1}$  for near-resonant charge transfer. This process is only exothermic by  $24 \text{ cm}^{-1}$ , due to differences in zero point energies between  $D\text{Br}^+$  and  $H\text{Br}^+$ . This rate constant is seven times larger than the rate constant,  $k_{1/2, v=0 \rightarrow 3/2, v=1} = 0.23 \times 10^{-10} \text{ cm}^3 \text{sec}^{-1}$ , for a nonresonant channel that is  $\sim 250 \text{ cm}^{-1}$  exothermic. The nonresonant charge transfer channel ( $1/2, v = 0 \rightarrow 3/2, v = 1$ ) may also be less efficient because the Franck-Condon factor for the 1-0 transition from the HBr ground state to its ion ground state is also smaller than the 0-0 transition.

The  $H\text{Br}^+$  product rotational state distributions resulting from reaction with  $D\text{Br}^+ {^2\Pi}_{1/2, v^+=0}$  exhibit interesting behavior (Figure 6). For  $H\text{Br}^+$  produced in the  ${^2\Pi}_{1/2, v^+=0}$  level the rotational distribution is nearly thermal at 300 K, if the  $e$  and  $f$   $\Lambda$ -splitting components are considered individually. In addition, the population of the  $e$  component on each  $J$  level is always twice as intense as the  $f$  component. When  $H\text{Br}^+$  is produced in the  ${^2\Pi}_{3/2, v^+=1}$  level, the rotational distribution is hotter than that observed for the  ${^2\Pi}_{1/2, v^+=0}$  level and the  $e$  and  $f$  levels are almost equally populated. The rotational distribution for the third channel,  ${^2\Pi}_{3/2, v^+=0}$ , is even hotter because the reaction is more exothermic; the  $e$  and  $f$   $\Lambda$ -splitting components are equally populated. These results may indicate that the near-resonant channel occurs through a long range interaction with some type of kinematic constraint that causes the ratio of the  $e$  and  $f$   $\Lambda$ -splitting components to differ from the statistically expected result of 2:1.

## 2. Theoretical Work: Selection Rules for the Photoionization of Diatomic Molecules

We have derived selection rules for the electric dipole allowed photoionization of diatomic molecules. Previous authors have derived selection rules for special cases.<sup>7-9</sup> We have derived selection rules for cases where the diatomic is in Hund's coupling case a, b, c, or d, and where the resultant ion can be in any of these coupling cases.<sup>10</sup>

These selection rules are derived by examining the transition dipole matrix element,  $\langle f | \mu | i \rangle$ , to find the cases where it is nonvanishing. The final state  $|f\rangle$  is equated with the wave function of the ion multiplied by the wavefunction of the photoelectron, where the photoelectron is treated as an expansion of partial waves in terms of its orbital

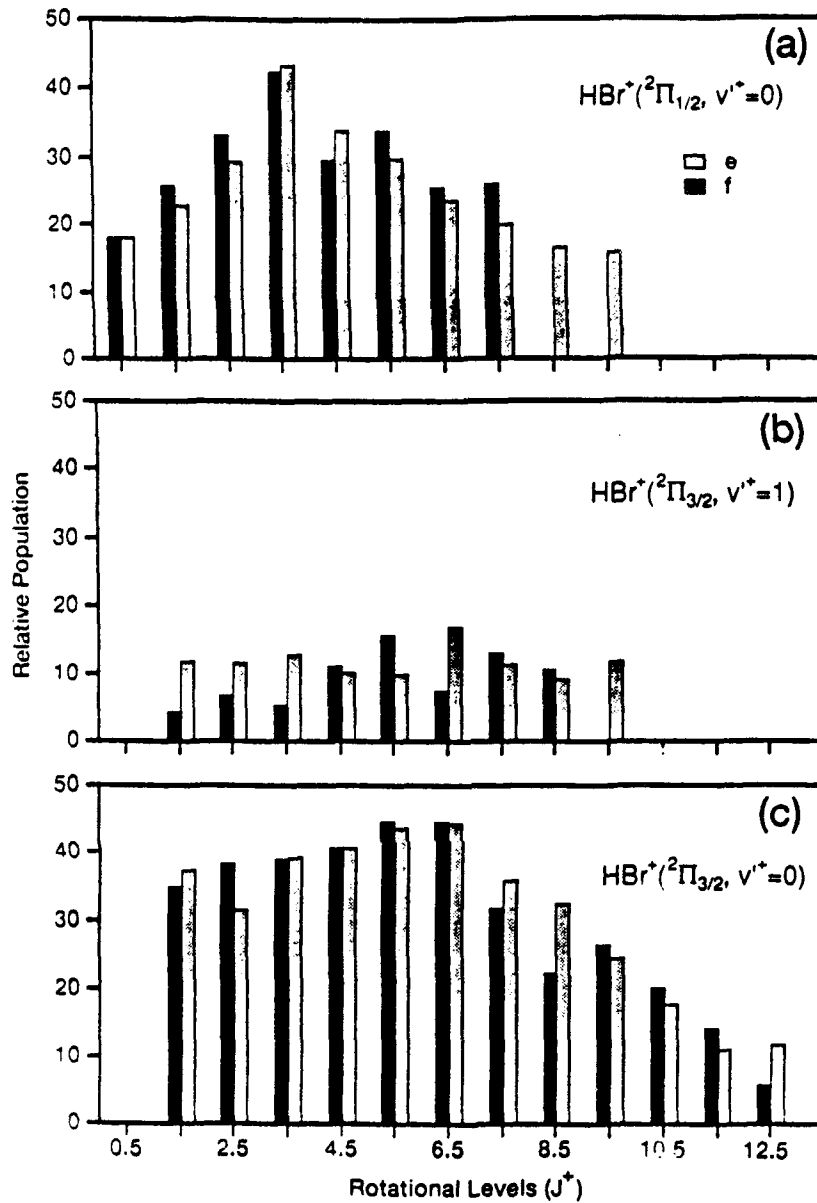


**Figure 6:** Rotational state distribution of product HBr<sup>+</sup> in <sup>2</sup>Π<sub>1/2</sub> v=0, <sup>2</sup>Π<sub>3/2</sub> v=1, and <sup>2</sup>Π<sub>3/2</sub> v=0, respectively produced by the charge transfer with DBr<sup>+</sup>.

angular momentum, *l*. The initial state, |i> is simply the wavefunction of the neutral molecule.

We have derived selection rules for the relevant quantum numbers for the various coupling cases as well as for total parity. In addition, in the case of homonuclear diatomics there are selection rules governing transitions between gerade and ungerade

states as well as symmetric and antisymmetric rotational levels. These selection rules are all summarized in the tables below:

Allowed transitions (final state)–(initial state)	Selection rules
all coupling cases	$\Delta J = l + \frac{1}{2}, l + \frac{1}{2}, \dots, -l - \frac{1}{2}$ $\Delta M_s = -m_s + \frac{1}{2}, -m_s + \frac{1}{2}, -m_s - \frac{1}{2}$ , and $-m_s - \frac{1}{2}$
case (a)–case (a) case (a)–case (b) case (b)–case (a) case (b)–case (b)	$\Delta \Lambda = -\lambda + 1, -\lambda, -\lambda - 1$ $\Delta S = \pm \frac{1}{2}$ $\Delta \Sigma = \pm \frac{1}{2}$
case (a)–case (a) case (c)–case (c) case (c)–case (a) case (a)–case (c) case (c)–case (b) case (b)–case (c)	$\Delta \Omega = -\lambda + \frac{1}{2}, -\lambda + \frac{1}{2}, -\lambda - \frac{1}{2}$ and $-\lambda - \frac{1}{2}$ or $\Delta \Omega = -\omega + 1, -\omega, -\omega - 1$
case (b)–case (b) case (d)–case (d)	$\Delta N = l + 1, l, \dots, -l - 1$ $\Delta M_s = -m_s + 1, -m_s, -m_s - 1$ $\Delta M_s = \pm \frac{1}{2}$
case (b)–case (d)	$N_c = N^+$ $l - l_s = \pm 1$

**Table 1:** Angular momentum selection rules for photoionization of a diatomic molecule.

Coupling case	Parity wave function	Parity
case (a) for $\Lambda = 0$ and $\Sigma = 0$	$(1/\sqrt{2})[(J\Omega M) n\Lambda\rangle S\Sigma\rangle + (-1)^p J - \Omega M\rangle n - \Lambda\rangle S - \Sigma\rangle]$ $ n J 0 M 0 S 0\rangle$	$(-1)^{J-S+p+\gamma}$ above with $p = 0$
case (b) for $\Lambda = 0$	$(1/\sqrt{2})[(N\Lambda M_s) n\Lambda\rangle + (-1)^p N - \Lambda M_s\rangle n - \Lambda\rangle] SM_s\rangle$ $ N 0 M_s 0 S\rangle$	$(-1)^{N+p+\gamma}$ above with $p = 0$
case (c) for $\Omega = 0$	$(1/\sqrt{2})[(J\Omega M) n\Omega\rangle + (-1)^p J - \Omega M\rangle n - \Omega\rangle]$ $ J 0 M\rangle n 0\rangle$	$J = \text{integer},$ $(-1)^{J+p+\gamma}$ $J = \text{half-integer},$ $(-1)^{J-1/2+p+\gamma}$ above with $p = 0$
case (d) for $\Lambda_c = 0$	$(1/\sqrt{2})[(N_c \Lambda_c M_{nc}) n\Lambda_c\rangle + (-1)^p N_c - \Lambda_c M_{nc}\rangle n - \Lambda_c\rangle]$ $ I_R m_R\rangle SM_s\rangle$ $ N_c 0 M_{nc}\rangle n 0\rangle I_R m_R\rangle SM_s\rangle$	$(-1)^{N_c+p+\gamma}$ above with $p = 0$

**Table 2:** Parity wave functions for the four different Hund's coupling cases.

Allowed transition (final state)–(initial state)	Selection rule
case (a)–case (a)	$(J^+ - J) - (S^+ - S) + (p^+ - p) + (s^+ - s) + l = \text{odd}$
case (a)–case (b)	$[N^+ - (J - S)] + (p^+ - p) + (s^+ - s) + l = \text{odd}$
case (b)–case (a)	$[(J^+ - S^+) - N] + (p^+ - p) + (s^+ - s) + l = \text{odd}$
case (b)–case (b)	$(N^+ - N) + (p^+ - p) + (s^+ - s) + l = \text{odd}$
case (a)–case (d)	$[(J^+ - S^+) - (N_c + l_R)] + (p^+ - p) + (s^+ - s) + l = \text{odd}$
case (b)–case (d)	$[N^+ - (N_c + l_R)] + (p^+ - p) + (s^+ - s) + l = \text{odd}$
case (c)–case (c)	$(J^+ - J) + (p^+ - p) + (s^+ - s) + l = \text{odd}^*$
case (b)–case (c)	$(N^+ - J) + (p^+ - p) + (s^+ - s) + l = \text{odd}$
case (a)–case (c)	$[(J^+ - S^+) - J] + (p^+ - p) + (s^+ - s) + l = \text{odd}$
case (c)–case (b)	$(J^+ - N^+) + (p^+ - p) + (s^+ - s) + l = \text{odd}^*$
case (c)–case (a)	$[J^+ - (J + S)] + (p^+ - p) + (s^+ - s) + l = \text{odd}^*$

\*Here we may also choose the coupled scheme for the photoelectron wave function because the ion core follows Hund's case (c). Then  $l$  is replaced by  $j - \frac{1}{2}$ .

**Table 3:** Parity selection rules for the photoionization of a diatomic molecule.

Selection Rule	Case
$(g/u) \leftrightarrow (g/u)$	$l = \text{odd}$
$(g/u) \leftrightarrow (u/g)$	$l = \text{even}$
$(s/a) \leftrightarrow (s/a)$	all cases

**Table 4:** Additional selection rules for homonuclear diatomics. Electronic states are classified as gerade(g) or ungerade(u). Rotational levels are classified as being symmetric or antisymmetric with respect to interchange of the nuclei.

### C. State-Selected Ion-Molecule Reactions

Although a large body of kinetic data<sup>11,12</sup> has been obtained under thermal conditions in flow reactors for ion-molecule reactions, the details of these reactions have not been studied nearly as extensively as their neutral counterparts. In an effort to understand the forces that drive ion-molecule reactions in greater detail, we are investigating the separate influences of ion reagent internal excitation and collision energy on the reaction outcome. The ion-molecule reaction studies are carried out with center-of-mass (CM) collision energies ranging from 0.5 to 10.0 eV in a quadrupole-octapole-quadrupole mass spectrometer, using ionic reagents state-selectively prepared by ( $n + 1$ ) REMPI.<sup>13,14</sup>

Previous ion-molecule studies in this laboratory<sup>15-18</sup> were performed on the  $\text{NH}_3^+ + \text{H}_2$ ,  $\text{NH}_3^+ + \text{CH}_4$ , and  $\text{NH}_3^+ + \text{ND}_3^+$  reactions using a tandem quadrupole mass spectrometer with a static collision cell located between the two quadrupole mass analyzers. Unfortunately, this experimental configuration precluded direct comparison of the signal intensity arising from different product channels and hence, the measurement of product branching ratios and reaction cross sections because forward-scattered product ions were detected more efficiently than side- and back-scattered products. Consequently, the previous work was limited to exploring the influence of vibrational excitation and collision energy only within a given product channel.

During the previous funding period, a radio frequency (rf) octapole ion guide<sup>19-24</sup> was constructed and installed in the collision cell region of our mass spectrometer, which is located between the two quadrupole mass analyzers, as illustrated in Figure 7. The octapole ion guide functions as an “ion pipe,” allowing nearly all of the product ions to be transported from the collision region to the second quadrupole mass analyzer, even when these product ions are scattered from the reactive collision with significant off-axis velocity components. With the discrimination in product detection removed, we can directly compare product intensities and determine product branching ratios and relative cross sections.

Figure 7 illustrates our current experimental configuration. Briefly, the state-selected ion beam is produced by ( $n + 1$ ) REMPI of a skinned molecular beam using the output of a frequency-doubled Nd:YAG pumped dye laser. The resulting ion beam is then focused and injected into the first quadrupole mass filter, which removes any fragments produced in the ionization process. The ion beam is accelerated to the desired collision energy as it enters the octapole ion guide which contains the neutral target gas.

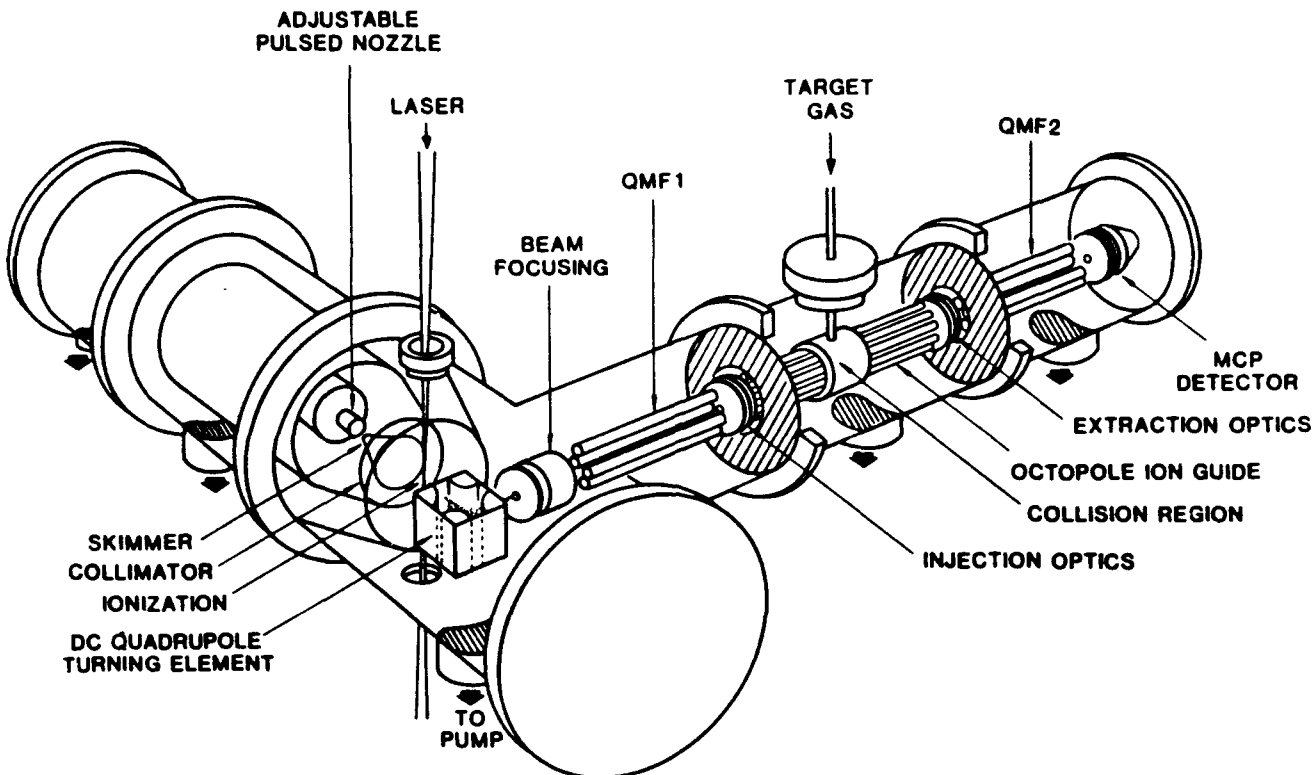
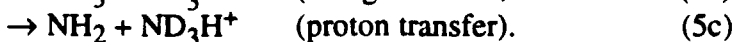
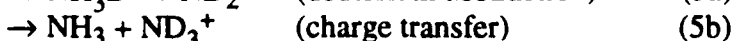


**Figure 7:** Ion-molecule quadrupole-octapole-quadrupole apparatus.

The thermal motion of the neutral reagent gas introduces a spread in the collision energy.<sup>25</sup> The pressure in the collision cell is sufficiently low to ensure single-collision conditions. The unreacted reagent ions and product ions, the latter being typically less than one per laser shot, are guided by the octapole from the collision cell region to the second quadrupole for mass analysis and subsequent detection.

### 1. Influence of Vibrational Excitation and Collision Energy on the $\text{NH}_3^+ + \text{ND}_3$ Reaction System

Since completing installation of the octapole ion guide, collision cell, and associated ion optics, we have investigated the effects of both vibrational excitation and collision energy on the ammonia ion/ammonia molecule reaction system. This system has three major product channels: hydrogen atom abstraction, charge transfer, and proton transfer. To distinguish between hydrogen atom abstraction and proton transfer channels, the neutral reagent is deuterium labeled:



The hydrogen abstraction and proton transfer channels have an overall reaction exothermicity of 0.79 eV, while charge transfer is essentially thermoneutral.

Under thermal conditions charge transfer proceeds with a rate constant of  $k \leq 4 \times 10^{-11} \text{ cm}^3\text{s}^{-1}$  whereas hydrogen abstraction or proton transfer occurs on nearly every collision ( $k = 1.9 \times 10^{-9} \text{ cm}^3\text{s}^{-1}$ ).<sup>26</sup> This system was one of the first ion-molecule reaction systems in which the effects of vibrational excitation were probed, albeit without preparation of the reagent ions in a single specified vibrational level.<sup>27</sup> Subsequent state-selected studies of this system have employed coincidence techniques<sup>28,29</sup> as well as state-selective ion preparation by REMPI.<sup>17</sup> As a result, the ammonia ion/ammonia reaction system is an excellent system for initial experiments using our recently modified apparatus; comparison of our results with the other data available on this system permitted characterization of the instrument performance.

The  $\text{NH}_3^+(v)$  reagent ion is prepared state-selectively with excitation in the  $v_2$  umbrella bending mode using (2 + 1) REMPI through the  $\tilde{\text{B}}$  or  $\tilde{\text{C}}'$  Rydberg state.<sup>13</sup> The ammonia ion is particularly attractive for studying the influence of vibrational excitation in chemical reactions; the ion can be prepared with up to 10 quanta in the umbrella mode, which corresponds to 1.23 eV of internal excitation. This broad range of accessible excitation results from the large geometry change in going from the pyramidal neutral to the planar ion. In addition, the possibility exists for exciting other vibrational modes in this polyatomic ion. For example, a progression in the umbrella mode built on the symmetric stretch ( $v_1 + nv_2$ ) can be excited in the  $\tilde{\text{C}}'$  state using REMPI,<sup>30</sup> which recent REMPI-PES work in this laboratory (Figure 1)<sup>31</sup> has demonstrated to produce  $\text{NH}_3^+$  ions cleanly with one quantum in the stretch and two or three quanta in the umbrella mode. This capability is the basis for ongoing work in this project looking at the effect on the system reactivity of exciting differing internal modes of the ion.

Two typical sets of parent and product ion TOF profiles for the ammonia reaction system with  $v_2, v = 0, 7$ , at a center-of-mass collision energy of 3.0 eV, are shown in Figure 8. Qualitative comparison of these raw data for a given set of reaction conditions suggest that fundamental differences exist between the product channel profiles. These TOF profiles reflect the projection of the product ion velocity component onto the ion beam axis of the instrument which passes through the center of the octapole ion guide. Qualitatively, the similarity between the reagent profile and the deuterium abstraction product suggests that the velocity vector of the reagent  $\text{NH}_3^+$  ion abstracting the deuterium atom from the neutral  $\text{ND}_3$  is relatively unchanged in the course of the reactive collision. In contrast, charge transfer and proton transfer have much broader TOF profiles; in both cases neutral reagent molecules that start with thermal velocities become

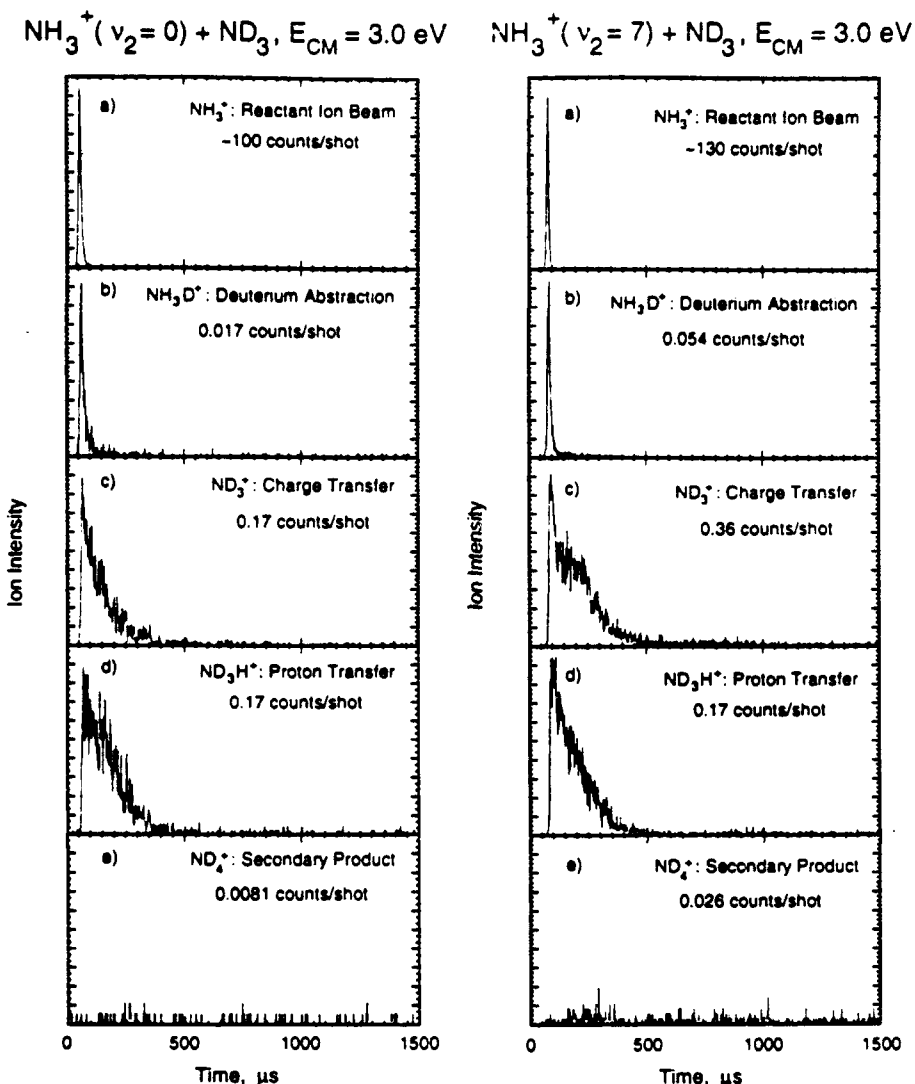


**Figure 8:** Raw data parent and product TOF profiles.

the detected charged products. Possible explanations for the broadened TOF distributions include significant kinetic energy release of the product ions, or perhaps incomplete transfer of the ion beam energy to the neutral reagent in the course of a reaction proceeding through a relatively short-lived complex. The TOF profiles also show sensitivity to the vibrational excitation in the reactant ion. At this point in our study of the TOF profiles, definitive conclusions cannot be made concerning their information content.

Product branching ratios were determined from the integrated TOF profiles. Figure 9 has the branching ratios plotted as a function of umbrella mode excitation in  $\text{NH}_3^+$  at three collision energies which cover the range investigated. These branching ratio plots indicate that the product channels of this system respond strongly to

vibrational excitation and collision energy. At the lowest collision energy of 1.0 eV CM (Figure 9a) the sensitivity to vibrational excitation is greatest, whereas at the highest collision energy (Figure 9c), little or no effect is evident as the umbrella mode excitation is increased. This decrease in system sensitivity to umbrella mode excitation is the result of translational energy overwhelming the initial vibrational excitation of the ion. Clearly, at collision energies of 5 eV or less, deuterium abstraction and charge transfer are enhanced by excitation of the  $v_2$  mode in  $\text{NH}_3^+$ , whereas proton transfer is suppressed. The product channels also show sensitivity to collision energy. At the lowest collision energy, proton transfer is the strongest channel. As the collision energy is increased, charge transfer, a negligible channel under thermal conditions,<sup>26</sup> becomes the dominant channel. At all collision energies deuterium abstraction is a relatively small channel, which accounts for less than 20% of the product ions.

In addition to measuring the product ion signal using single ion counting, we also record the analog intensity of the unreacted  $\text{NH}_3^+$ , which enables us to determine relative

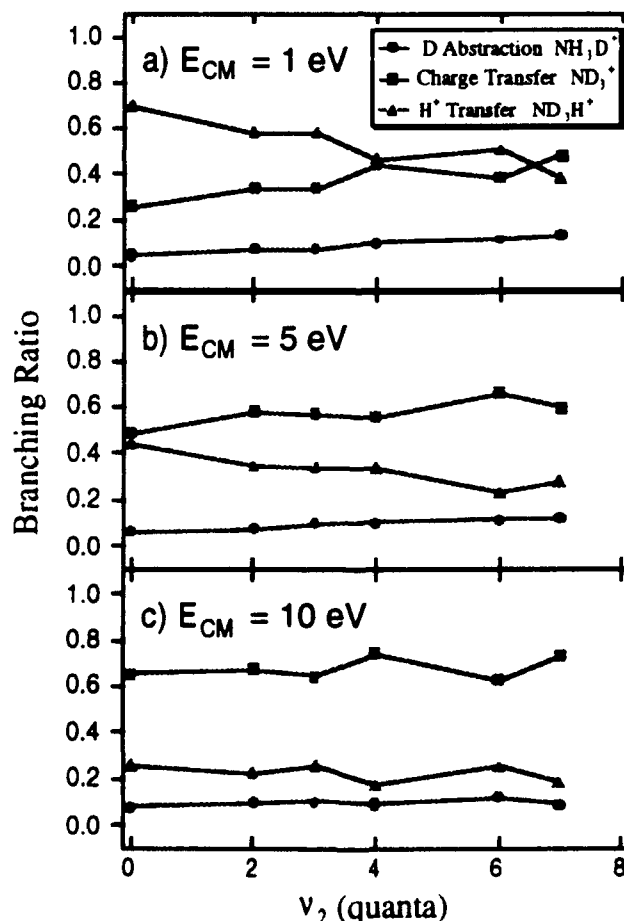


**Figure 9:** Branching ratio vs.  $v_2$  quanta at three collision energies:  
a) 1 eV, b) 5 eV, and c) 10 eV.

cross sections. The relative cross section measurements allow us to see directly which channels are becoming suppressed or enhanced as a function of either collision energy or vibrational excitation. Figure 10 shows the relative cross sections of each of the primary product channels as a function of reagent ion umbrella mode excitation for three collision energies. Once again the effects of vibrational excitation are strongest at the lowest collision energy, 1.0 eV, and are attenuated at higher collision energies, particularly for proton transfer. At 1.0 eV deuterium abstraction (Figure 10a) is enhanced by a factor of three in going from  $v = 0$  to  $v = 7$  in the umbrella mode. The charge transfer channel (Figure 10b) increases by nearly a factor of two, while proton transfer (Figure 10c) is reduced by a factor of two as the excitation in  $v_2$  is increased from  $v = 0$  to  $v = 7$ . Similar trends were observed by Conaway *et al.*<sup>17</sup>; however, they observed much greater enhancement of deuterium abstraction with increasing vibrational excitation.

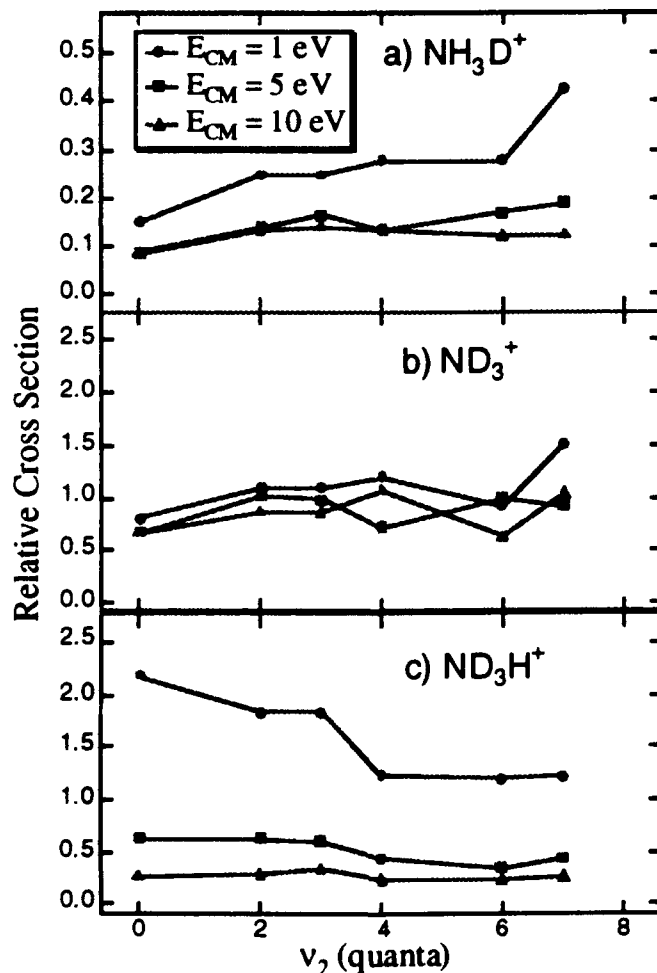


**Figure 10:** Relative cross section vs.  $v_2$  quanta at three collision energies, 1 eV, 5 eV, and 10 eV, for the product channels: a) deuterium abstraction, b) charge transfer, and c) proton transfer.

## 2. Discussion

Our results allow us to critique and extend the current models for the behavior of the ammonia ion/ammonia system. The behavior of the proton transfer channel (5c) has been explained by a direct model<sup>17,29,32</sup> in which a proton passes from the NH<sub>3</sub><sup>+</sup> ion to the central nitrogen atom in the neutral reagent (Figure 11). Excitation of the umbrella mode results in motion orthogonal to the reaction coordinate for proton transfer as illustrated in Figure 11. It might be expected that this process would be hindered by such motion resulting in a decrease in the relative cross sections as the umbrella mode excitation is increased. Our results shown in Figure 10c are consistent with such a model, showing a factor of two drop as excitation is increased from v<sub>2</sub>=0 to v<sub>2</sub>=7.

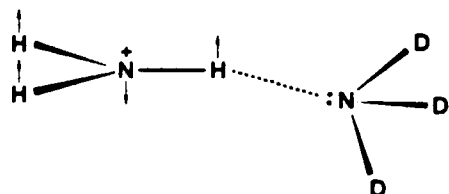


**Figure 11:** NH<sub>3</sub><sup>+</sup> + ND<sub>3</sub> proton transfer model.

As mentioned above, both charge transfer (5b) and deuterium abstraction (5a) are enhanced by increasing the vibrational excitation of the NH<sub>3</sub><sup>+</sup> ion. In charge transfer an electron must hop from the nonbonding orbital on the nitrogen of the neutral ND<sub>3</sub> to the half-filled orbital on the NH<sub>3</sub><sup>+</sup> (Figure 12). Orbital overlap arguments suggest that an approach geometry which has the nonbonding orbital on the ion and neutral pointed toward each other would be most favorable for electron transfer. This appears to be a favorable geometry for reagent approach because the dipole of the neutral is directed toward the charge. It has been suggested that the enhancement in charge transfer results from the increase in Franck-Condon overlap between the ion and neutral with increasing excitation in the umbrella mode; however, the enhancement is smaller than expected if Franck-Condon overlap was the governing factor, considering that the Franck-Condon factors increase by a factor of 30 in going from v = 0 to v = 5 in the umbrella mode. Baer and Murray<sup>28</sup> have suggested that nonresonant channels play an important role in charge transfer. The enhancement of this channel with increasing internal excitation of the ionic reagent and collision energy may simply reflect a shorter interaction time between the reagents. The reactive complex can fall apart after the electron has jumped but before a heavier particle can be transferred.

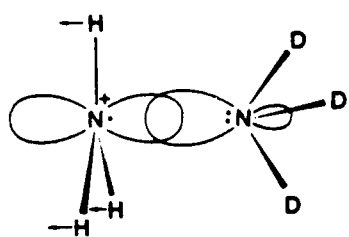


**Figure 12:**  $\text{NH}_3^+$  +  $\text{ND}_3$  charge transfer model.

Several models have been proposed to explain the enhancement of the deuterium abstraction channel. Figure 13 illustrates deuterium transfer, which can be viewed either as one-step transfer of an atom or a two-step process consisting of electron transfer followed by proton transfer. In the direct atom transfer model<sup>17,32</sup> the umbrella bending motion is viewed as motion along the reaction coordinate. In order for a fourth H/D atom to bind to the central nitrogen atom the ion must bend from its planar equilibrium structure. In contrast, the two-step model<sup>29</sup> attributes the enhancement to promotion of the initial charge transfer step by improved Franck-Condon overlap between the ion and neutral at higher vibrational excitations. Currently, our data do not allow us to distinguish between these two models.

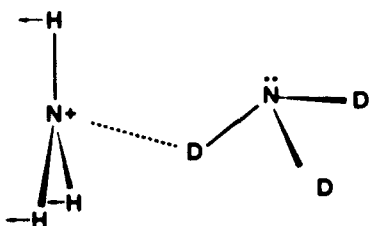


**Figure 13:**  $\text{NH}_3^+$  +  $\text{ND}_3$  deuterium abstraction model.

## References

1. C. H. Kuo, C. G. Beggs, P. R. Kemper, M. T. Bowers, D. J. Leahy, and R. N. Zare, *Chem.Phys.Lett.* **163**, 291 (1989).
2. D. J. Leahy, R. K.L., and R. N. Zare, *J.Chem.Phys.* **95**, 1757 (1991).
3. K. L. Reid, D. J. Leahy, and R. N. Zare, *J.Chem.Phys.* **95**, 1746 (1991).
4. H. Rudolph and V. McKoy, *J. Chem. Phys.* **91**, 2235 (1989).
5. A. Viggiano (personal communication).
6. J. Xie and R. N. Zare, in preparation.
7. S. N. Dixit and V. McCoy, *Chem. Phys. Lett.* **128**, 49 (1986).
8. S. T. Pratt, P. M. Dehmer, and J. L. Dehmer, *J. Chem. Phys.* **78**, 1983 (1983).
9. M. A. O'Halloran, S. T. Pratt, P. M. Dehmer, and J. L. Dehmer, *J. Chem. Phys.* **87**, 3288 (1987).
10. J. Xie and R. N. Zare, *J. Chem. Phys.* **93**, 3033 (1990).
11. D. L. Albritton, *Atomic Data and Nuclear Data Tables* **22**, 1 (1978).
12. Y. Ikezoe, S. Matsuoka, M. Takebe, and A. Viggiano, *Gas-phase ion-molecule reaction rate constants through 1986*, (Ion Reaction Research Group of The Mass Spectroscopy Society of Japan, Tokyo, 1987).
13. W. E. Conaway, R. J. S. Morrison, and R. N. Zare, *Chem. Phys. Lett.* **113**, 429 (1985).
14. T. Ebata and R. N. Zare, *Chem. Phys. Lett.* **130**, 467 (1986).
15. R. J. S. Morrison, W. E. Conaway, and R. N. Zare, *Chem. Phys. Lett.* **113**, 435 (1985).
16. R. J. S. Morrison, W. E. Conaway, T. Ebata, and R. N. Zare, *J. Chem. Phys.* **84**, 5527 (1986).
17. W. E. Conaway, T. Ebata, and R. N. Zare, *J. Chem. Phys.* **87**, 3453 (1987).
18. W. E. Conaway, T. Ebata, and R. N. Zare, *J. Chem. Phys.* **87**, 3447 (1987).
19. E. Teloy and D. Gerlich, *Chem. Phys.* **4**, 417 (1974).
20. S. L. Anderson, F. A. Houle, D. Gerlich, and Y. T. Lee, *J. Chem. Phys.* **75**, 2153 (1981).
21. K. M. Ervin and P. B. Armentrout, *J. Chem. Phys.* **83**, 166 (1985).
22. T. M. Orlando, B. Yang, and S. L. Anderson, *J. Chem. Phys.* **90**, 1577 (1989).
23. J. D. Shao and C. Y. Ng, *J. Chem. Phys.* **84**, 4317 (1986).
24. C. Liao, J. Shao, R. Xu, G. D. Flesch, Y. Li, and C. Y. Ng, *J. Chem. Phys.* **85**, 3874 (1986).
25. P. J. Chantry, *J. Chem. Phys.* **55**, 2746 (1971).
26. W. T. Huntress Jr., M. M. Mosesman, and D. D. Elleman, *J. Chem. Phys.* **54**, 843 (1971).
27. W. A. Chupka and M. E. Russell, *J. Chem. Phys.* **48**, 1527 (1968).
28. T. Baer and P. T. Murray, *J. Chem. Phys.* **75**, 4477 (1981).
29. S. Tomoda, S. Suzuki, and I. Koyano, *J. Chem. Phys.* **89**, 7268 (1988).
30. P. J. Miller, S. D. Colson, and W. A. Chupka, *Chem. Phys. Lett.* **145**, 183 (1988).
31. D. Leahy and R. N. Zare, unpublished results.
32. W. J. Chesnavich and M. T. Bowers, *Chem. Phys. Lett.* **52**, 179 (1977).

## PUBLICATIONS

- C. -H. Kuo, C. G. Beggs, P. R. Kemper, M. T. Bowers, D. J. Leahy, and R. N. Zare, "Experimental Measurement of the Radiative Lifetime of NO<sup>+</sup> ( $X\ ^1\Sigma^+$ , v=1, 2, and 3)," *Chem. Phys. Lett.* **163**, 291-296 (1989).
- J. Xie and R. N. Zare, "Selection Rules for the Photoionization of Diatomic Molecules," *J. Chem. Phys.* **93**, 3033-3038 (1990).
- K. L. Reid, D. J. Leahy, S. W. Allendorf, and R. N. Zare, "Effect of Breaking Cylindrical Symmetry on Photoelectron Angular Distributions Resulting from Resonance-Enhanced Two-Photon Ionization," *Inst. Phys. Conf. Ser. No. 114; Section 8, RIS 90, Proceedings of the Fifth International Symposium on Resonance Ionization Spectroscopy and Its Applications*, 345-350 (1991).
- K. L. Reid, D. J. Leahy, and R. N. Zare, "Effect of Breaking Cylindrical Symmetry on Photoelectron Angular Distributions Resulting from Resonance-Enhanced Two-Photon Ionization," *J. Chem. Phys.* **95**, 1746-1756 (1991).
- D. J. Leahy, K. L. Reid, and R. N. Zare, "Complete Description of Two-Photon (1+1') Ionization of NO Deduced from Rotationally Resolved Photoelectron Angular Distributions," *J. Chem. Phys.* **95**, 1757-1767 (1991).
- J. Xie and R. N. Zare, "Determination of Absolute Thermal Rate Constants for the Charge-Transfer Reaction DBr<sup>+</sup> ( $^2\Pi_{1/2}$ , v<sup>+</sup>) + HBr  $\rightarrow$  HBr<sup>+</sup> ( $^2\Pi_{1/2}$ , v'<sup>+</sup>) + DBr," *J. Chem. Phys.* **96**, 4293-4302 (1992).
- L. A. Posey, R. D. Guettler, B. A. Keller, and R. N. Zare, "Influence of Vibrational Excitation and Collision Energy on the Ion-Molecule Reaction NH<sub>3</sub><sup>+</sup> (v<sub>2</sub>) + ND<sub>3</sub>," *J. Chem. Phys.* (submitted).

## PERSONNEL

### *Graduate Students*

Sarah W. Allendorf, Ph.D. 03/13/89, "Angle- and Energy-Resolved Photoelectron Spectroscopy: A Probe of Photoionization Dynamics."

Richard Green

Robert D. Guettler

David J. Leahy

Jinchun Xie

### *Postdoctoral Scholars*

Dr. Beat A. Keller

Dr. Nicholas J. Kirchner

Dr. Lynmarie A. Posey

Dr. Katharine L. Reid